First-principles studies of complex magnetism in Mn nanostructures on the Fe(001) surface

R. N. Igarashi,[1] A. B. Klautau,[2] R. B. Muniz,[3] B. Sanyal,[4] and H. M. Petrilli[1]
[1]*Instituto de Física, Universidade de São Paulo, CP 66318, 05315-970, São Paulo, SP, Brazil*
[2]*Faculdade de Física, Universidade Federal do Pará, Belém, PA, Brazil*
[3]*Instituto de Física, Universidade Federal Fluminense, 24210-340, Niterói, RJ, Brazil*
[4]*Department of Physics and Astronomy, Uppsala University, Box 516, 75120 Uppsala, Sweden*
(Received 17 November 2011; published 31 January 2012)

The magnetic properties of Mn nanostructures on the Fe(001) surface have been studied using the noncollinear first-principles real space–linear muffin-tin orbital–atomic sphere approximation method within density-functional theory. We have considered a variety of nanostructures such as adsorbed wires, pyramids, and flat and intermixed clusters of sizes varying from two to nine atoms. Our calculations of interatomic exchange interactions reveal the long-range nature of exchange interactions between Mn-Mn and Mn-Fe atoms. We have found that the strong dependence of these interactions on the local environment, the magnetic frustration, and the effect of spin-orbit coupling lead to the possibility of realizing complex noncollinear magnetic structures such as helical spin spiral and half-skyrmion.

DOI: 10.1103/PhysRevB.85.014436 PACS number(s): 75.75.−c, 73.22.−f, 75.10.−b

I. INTRODUCTION

The magnetic interaction between an antiferromagnet and a ferromagnet drives the essential physics underlying the magnetic properties of the principal constituents of magnetic storage exchange-bias devices. However, a complete microscopic understanding of the mechanisms that occur at the ferromagnetic-antiferromagnetic interface is still a challenge due to the presence of various types of chemical and magnetic disorder. In this regard, Mn overlayers on the Fe(001) surface constitute interesting systems for investigating magnetic couplings across a ferromagnetic-antiferromagnetic interface, and exhibit an intricate interdependence between magnetism and film thicknesses. Experimental results reveal that for Mn films with two or more atomic layers, the Mn layers are antiferromagnetically (AF) coupled to each other, but ferromagnetically (FM) coupled to the Fe layer at the interface between Mn and Fe.[1–5] However, for a single-layer coverage, the Mn layer has an in-plane canted antiferromagnetic structure in which the Mn moments are nearly perpendicular to Fe substrate magnetization,[6] in agreement with the negligible observed value of the Mn layer net magnetization.[6–8] On the contrary, for submonolayer coverages of Mn on Fe(001), experimental studies show that the Mn moments couple ferromagnetically among themselves, but are antiparallel to the underlying Fe magnetization.[1,7,8] In addition, for Mn films grown on an Fe(001) surface with a monoatomic step, a noncollinear magnetic order appears around the defect.[3,9–11] Regarding the crystal structures, ultrathin films of Mn (up to two monolayers) on Fe(001) stabilizes in a body-centered tetragonal (bct) structure, close to the bcc Fe structure.[12–15] For thicker Mn overlayers, the distance between the Mn atomic planes increases.[13,16] Moreover, the presence of interface diffusion with Mn atoms incorporated in the Fe surface layer makes the problem even more complicated.[7,16,17]

Theoretical studies on the magnetic structure of Mn thin films adsorbed on Fe(001) substrates have been carried out for the past few years.[6,9,18–26] Nevertheless, only a few studies have been carried out for supported Mn clusters on a bcc Fe(001) surface.[19,27] With the experimental techniques now available, nanowires and nanostructures may be deposited on magnetic and nonmagnetic surfaces in a controlled fashion, and their fundamental magnetic properties can be explored with the use of advanced experimental methods.[28–34]

From the above discussions, it is quite evident that the magnetic interactions at the interface between Mn and Fe have a very rich variety depending on the geometry and local environment. Particularly, the study of the nanostructures of Mn supported on Fe is quite fascinating. In this article, we present first-principles calculations of the electronic structure and magnetic properties of Mn nanowires as well as two- and three-dimensional nanoislands supported on the Fe(001) surface. Our investigation has also been motivated by the possible existence of bi- and multistable magnetic configurations in these systems, with total energies differing by few milli-electron-volts.[35] These nanostructures are promising candidates for nanoscale magnetic data storage units, and recent theoretical studies have explored the possibility of using electric[36] and magnetic[37] fields to switch them from a local magnetic stable configuration to another.

We investigate effects of atomic interdiffusion and local structural features on the magnetic characteristics of Mn nanostructures on Fe(001) surfaces. We also discuss the role of the long-range nature of the exchange couplings, their dependence on the local environment, e.g., the number and type of neighbors, and their influences on the ground-state local magnetic configurations. Interestingly, we find the existence of collinear and intriguing noncollinear magnetic arrangements (e.g., spin spiral and half-skyrmion) with total energies that are nearly degenerate. Based on the calculations of exchange coupling constants, we discuss the magnetic orderings of several Mn nanostructures adsorbed on Fe(001), ranging from a single Mn adatom to ultrathin films of Mn supported on Fe(001).

II. COMPUTATIONAL DETAILS

Our calculations have been performed using the first-principles, self-consistent RS-LMTO-ASA (real space–linear

muffin-tin orbital–atomic sphere approximation) method,[38,39] which is based on the LMTO-ASA formalism,[40] and employs the recursion method[41] to solve the eigenvalue problem directly in real space. The RS-LMTO-ASA method has been generalized to describe noncollinear magnetism.[42,43] The calculations presented here are fully self-consistent and performed within the local spin-density approximation (LSDA).[44] In this study, we have considered Mn nanostructures with different geometries supported on a Fe(001) surface.

The Fe(001) surface has been modeled by a cluster containing ∼10 000 atoms positioned in a bcc lattice with the experimental lattice parameter of Fe. In the recursion method, the continued fraction has been calculated exactly up to 20 recursion levels and then appended with the Beer-Pettifor terminator.[45] In order to provide a basis for the wave function in the vacuum outside the surface and to treat charge transfers correctly, we included two layers of empty spheres above the Fe surface. The calculations of the Mn nanostructures have been performed by embedding the clusters as a perturbation on the self-consistently converged Fe(001) surface. The Mn sites and the first and second nearest neighbors of Fe (or empty spheres) atoms around the defect were recalculated self-consistently, with size varying from 10 up to 78 sites, while the potential parameters for all other sites far from the Mn cluster were kept unchanged.

We have performed calculations with and without structural relaxations. In the latter we consider that the Mn atoms occupy the unrelaxed hollow positions, assuming the experimental lattice parameter of the Fe substrate. In the former we inspect inward and outward perpendicular relaxations to the Fe(001) surface of 2% and 6%. These choices are based on experimental results, where it was observed that Mn grows on Fe(001) in a bct structure, with the in-plane lattice parameter of Fe (2.87 Å), and out-of-plane distances ($d_\perp$) that vary with the Mn film thickness. For example, in ultrathin films with up to two monolayers of Mn/Fe(001), the Fe-Mn interplanar distance is $d_\perp^{\mathrm{FeMn}} \approx 1.4$ Å, whereas the separation between the Mn layers is $d_\perp^{\mathrm{MnMn}} \approx 1.5$ Å.[12–15] Fully relativistic calculations forcing a magnetic collinear configuration have been carried out by taking into account the spin-orbit interaction in each variational step. Our results show that the atomic orbital moments are rather small, being less than $0.04\mu_B$/atom and $0.1\mu_B$/atom for Mn and Fe atoms, respectively. For noncollinear magnetic arrangements, we also performed calculations with spin-orbit coupling. For a particular system of a nanowire with nine atoms, we also performed noncollinear calculations without spin-orbit coupling, in order to extract the effect of this interaction on the magnetic configuration of the system.

The Heisenberg exchange interaction parameters J_{ij} have been calculated employing the formula of Liechtenstein *et al.*,[46] as implemented in the RS-LMTO-ASA method.[47] The obtained values of J_{ij} are then used to analyze, on a qualitative level, the competition between nearest and next-nearest interactions, as well as the effect of frustration in the magnetic orderings explored in our full noncollinear calculations. The positive (negative) value of J_{ij} indicates a ferromagnetic (antiferromagnetic) coupling.

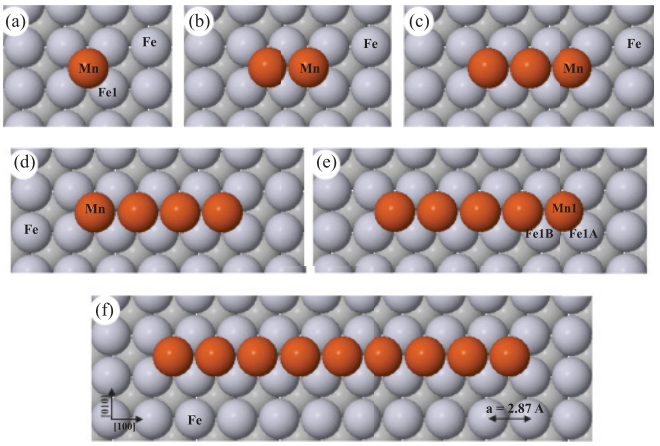

FIG. 1. (Color online) Finite linear chains of Mn atoms adsorbed on bcc Fe(001) surface. The red (dark) and gray (light) balls indicate Mn and Fe atoms, respectively.

III. RESULTS AND DISCUSSIONS

A. Mn nanowires on Fe(001)

1. Collinear structures

In Fig. 1 we show the geometries of various finite linear chains of Mn atoms adsorbed on bcc Fe(001) along the [100] direction. Each Mn atom, in this case, has only Fe atoms as its first nearest neighbors, though its next nearest neighbors can be either Mn or Fe atoms, where the closest distance between Mn atoms is equal to the bcc Fe lattice parameter ($a = 2.87$ Å) and the configurations are denoted by Mn_n/Fe(001). We have performed calculations for different collinear magnetic configurations of the Mn nanostructures, assuming that the Fe substrate is always in a ferromagnetic state. We consider the following cases: (i)-(FM), where all Mn and Fe magnetic moments are ferromagnetically aligned; (ii)-(AF), where all Mn moments are ferromagnetically aligned, but antiferromagnetically aligned to the Fe moments; and (iii), where all Mn magnetic moments are antiferromagnetically aligned to each other. In (iii) we have examined three situations: chains with even number of Mn atoms (iii.1)-(FI1), where the net Mn magnetization is virtually zero; and chains with odd numbers of Mn atoms, where there is always one unpaired Mn moment leading to a finite Mn chain net magnetization that may be aligned either parallel (iii.2)-(FI2) or antiparallel (iii.3)-(FI3) to the Fe substrate magnetization.

Our calculations show that the spin contributions to the Mn magnetic moments may vary considerably. For case (i)-(FM), we obtained $m_{\mathrm{Mn}} = 3.4\mu_B$ for a single Mn adatom, $m_{\mathrm{Mn}} \approx 3.3\mu_B$ for Mn atoms located at the tips of the chains, and $m_{\mathrm{Mn}} \approx 3.2\mu_B$ for Mn central sites. Our results for Mn sites coupled antiferromagnetically to the substrate are systematically larger than those obtained in case (i)-(FM), ranging from $m_{\mathrm{Mn}} \approx 3.5\mu_B$ for Mn atoms located at the chain's tips to $m_{\mathrm{Mn}} \approx 3.6\mu_B$ for Mn atoms at inner sites. The corresponding values for surface Fe atoms with only one and two Mn nearest neighbors are $m_{\mathrm{Fe}} \approx 2.6\mu_B$ and $m_{\mathrm{Fe}} \approx 2.2\mu_B$, respectively. For subsurface Fe atoms we found $m_{\mathrm{Fe}} \approx 2.1\mu_B$.

We shall start by analyzing the magnetic configuration of a single Mn atom adsorbed on Fe(001) [Fig. 1(a)] in comparison with a substitutional Mn impurity embedded in the Fe surface layer. We find that the Mn adatom couples ferromagnetically to Fe substrate moments, whereas the Mn substitutional impurity couples antiferromagnetically.

The difference in energy between the (i)-(FM) and (ii)-(AF) configurations is ~ 13 meV/atom for the adatom and $\sim$29 meV/atom for the impurity case. These results are in agreement with previous *ab initio* calculations.[27] In both cases the magnetic ordering is a consequence of the rather long-range exchange coupling between the Mn and Fe atoms. The value of the exchange coupling parameter (J_{ij}) between the Mn adatom and its four Fe nearest neighbors [Fe1(S)] localized in the surface layer, calculated from the ferromagnetic configuration, is $J_{\mathrm{Mn-Fe1}(S)} = -2.7$ meV. However, the coupling with its second-nearest-neighbor Fe atoms [Fe2(S-1)] located in the subsurface layer (S-1) is much stronger and positive: $J_{\mathrm{Mn-Fe2}(S-1)} = +15$ meV. For Fe atoms situated at larger distances $J_{\mathrm{Mn-Fe}}$ is much smaller ($\leqslant$0.4 meV). The values of J_{ij} between the Mn substitutional impurity and its four nearest-neighbor Fe atoms located in the subsurface layer and in the surface layer are -10.9 meV and 6.8 meV, respectively. In its most stable configuration the Mn substitutional impurity has a spin magnetic moment $m_{\mathrm{Mn}} = -3.75\mu_B$. Its Fe neighbors in the surface layer have $m_{\mathrm{Fe1}(S)} = 2.89\mu_B$, and those in the subsurface layer have $m_{\mathrm{Fe2}(S-1)} = 1.90\mu_B$.

For a Mn dimer adsorbed on Fe(001) [Fig. 1(b)], we found that the energy differences between the magnetic configurations (i)-(FM), (ii)-(AF), and (iii.1)-(FI1) are relatively small: $\sim$3 meV/atom. For a Mn trimer and for longer Mn nanochains we obtained that several collinear magnetic configurations correspond to energy local minima, representing stable and metastable states whose total energies differ by just a few meV/atom. Nevertheless, for chains with an even number of Mn atoms we found that the magnetic configuration with lowest energy is (iii.1)-(FI1), and for those with an odd number of Mn atoms the lowest energy magnetic configuration is (iii.2)-(FI2).

We have also performed calculations for a Mn dimer and a Mn trimer placed along the [110] direction. Here, the Mn interatomic distance is $d = \sqrt{2}a$; we also obtained that both configurations (i)-(FM) and (iii.1)-(FI1) are magnetically stable for the dimer, and that (iii.2)-(FI2) is the most stable configuration for the trimer, but with total energy very close to that of other collinear magnetic states.

In order to shed some light on these results, we show in Fig. 2 some calculated values of the exchange coupling parameters between the Mn atoms ($J_{\mathrm{Mn-Mn}}$) as well as between Mn and Fe atoms ($J_{\mathrm{Mn-Fe}}$) for various Mn chains. All values were obtained from the FM configuration (i). We note that the coupling $J_{\mathrm{Fe-Fe}}$ between nearest-neighbor Fe atoms is always strong and positive, and decays relatively fast for more distant neighbors. However, we can see in Fig. 2 that $J_{\mathrm{Mn-Mn}}$ and $J_{\mathrm{Mn-Fe}}$ are still large for interatomic separations beyond nearest neighbors. We also note that in these systems, $J_{\mathrm{Mn-Fe}}$ depends not only on the interatomic distance, but strongly on the number of Mn atoms that are first nearest neighbors of the Fe atom. Even the sign of $J_{\mathrm{Mn-Fe}}$ changes when the

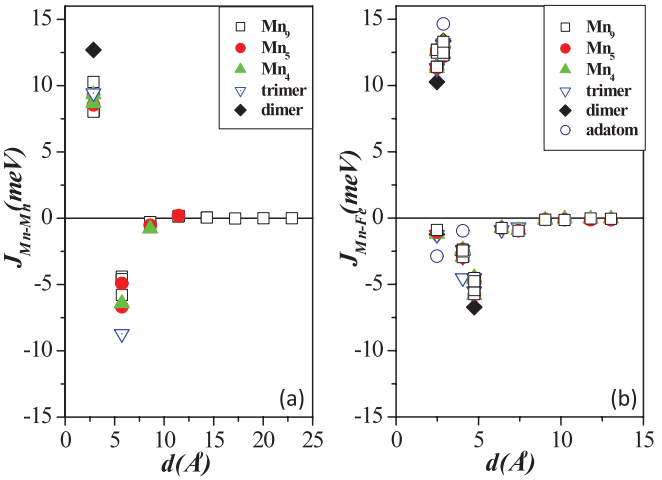

FIG. 2. (Color online) Exchange coupling parameters (a) between Mn atoms, $J_{\mathrm{Mn-Mn}}$, and (b) Mn and Fe atoms, $J_{\mathrm{Mn-Fe}}$, according to Fig. 1.

number of Mn nearest neighbors of the Fe atom varies. For example, for Fe atoms with only one Mn atom as a nearest neighbor the value of $J_{\mathrm{Mn-Fe}}$ is negative, otherwise $J_{\mathrm{Mn-Fe}}$ is positive. For a Mn chain with five atoms, the exchange coupling between a Mn atom located at the tip of the Mn chain and its first-nearest-neighbor Fe atom situated in the surface layer is $J_{\mathrm{Mn1-Fe1}A} = -1.4$ meV (note that this Fe atom has only one Mn nearest neighbor), whereas the coupling between this same Mn atom and the other nearest-neighbor Fe (which has two Mn nearest neighbors) is $J_{\mathrm{Mn1-Fe1}B} = 10.9$ meV [see Fig. 1(e)]. Also, the coupling between a Mn atom and its second-nearest-neighbor Fe atoms is always FM, and of the same order of magnitude as (or somewhat larger than) the coupling with the nearest-neighbor Fe atoms, though with different sign in some cases. Therefore, a simple Heisenberg model which takes into account nearest-neighbor interactions only is clearly inappropriate to describe these systems. A sensible analysis of their magnetic properties requires a much more elaborated approach, in view of the range of the pairwise exchange interactions and their dependence on the atomic neighborhoods.

We investigate the effect of structural relaxations on the magnetic properties of some Mn nanostructures adsorbed on Fe(001), namely a single Mn atom, a Mn dimer, and a Mn trimer. We have recalculated their electronic structure, magnetic moments, and most stable magnetic configurations considering variations of $\pm 6\%$ and $\pm 2\%$ in the distance between the Mn nanostructure and the Fe substrate. Our results show that the calculated magnetic moments do not change appreciably by such relaxations. The Mn local magnetic moments change by less than $0.1\mu_B$, and the Fe moments located in the surface layer vary in the range of 0.05 to $0.15\mu_B$, with values that decrease under compression and increase with expansion. The magnetic moments of Fe atoms with a greater number of Mn nearest neighbors present larger variations, and those located in the subsurface layer do not change significantly. The exchange coupling parameters $J_{\mathrm{Mn-Mn}}$ and $J_{\mathrm{Mn-Fe}}$, on the other hand, are strongly affected by such relaxations, but no changes in their signs were observed.

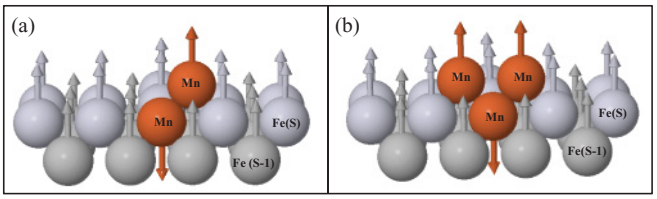

FIG. 3. (Color online) Magnetic configurations for Mn (a) dimer and (b) trimer, where one Mn atom is embedded at the Fe surface layer and the other one or two atoms are located above the Fe(001) surface, at a first neighbor distance.

Therefore, the magnetic configurations of the dimer and trimer are maintained even when considering relaxations of ±6%. The only exception is for an outward relaxation of 6% for the Mn adatom on Fe(001), where the FM and the AFM configurations become almost degenerate.

We have also analyzed the effect of Mn interdiffusion by calculating the magnetic configurations of a Mn dimer and trimer where we consider one Mn atom of the nanostructure as a substitutional impurity in the Fe surface layer, and the others as adatoms on the Fe surface, positioned as first nearest neighbors. The coupling between the embedded and adsorbed Mn atoms are strong and antiferromagnetic. We found $J_{\mathrm{Mn-Mn}} = -102$ meV and $J_{\mathrm{Mn-Mn}} = -54$ meV for the Mn dimer and trimer, respectively. These interactions are much stronger than any other Mn-Mn and Mn-Fe interactions, and lead to the most stable magnetic configurations shown in Fig. 3. The energy differences between these states and the other possible collinear configurations are always larger than 20 meV/atom. Our results are in agreement with x-ray magnetic circular dichroism measurements, which indicate that the moments of Mn atoms incorporated in the Fe(001) surface are coupled antiparallel to the direction of the Fe moments.[7]

The existence of several stable collinear magnetic orderings for adsorbed Mn nanochains on Fe(001), without interdiffusion, is possibly related to the presence of stable spin textures with nontrivial topology.[48–51] Similarly, previous theoretical results reveal noncollinear magnetic configurations for one and two[19] and for six[37] Mn layers supported on Fe(001).

2. *Noncollinear results*

The long-range nature and competitions between FM and AFM pairwise exchange interactions suggest that the magnetic configurations of Mn nanostructures adsorbed on Fe(001) may deviate from collinear arrangements. We have explored this possibility by performing calculations for the Mn nanostructures depicted in Figs. 1(c)–1(f), taking into account spin-orbit coupling and allowing noncollinear magnetic configurations to be realized. Our results are shown in Figs. 4(a)–4(d), where the Fe substrate moments (not shown) are oriented out of plane.

They may be viewed as having a Mn canted FM-like ordering, where an AF alignment between Mn and nearest-neighbor Fe spins is favored. This picture agrees with the experimental results and interpretations reported for low Mn coverages on the Fe(001) surface.[1,7,8]

It is worth noting that the energies of the noncollinear states shown in Figs. 4(a)–4(d) are quite similar to the collinear ones,

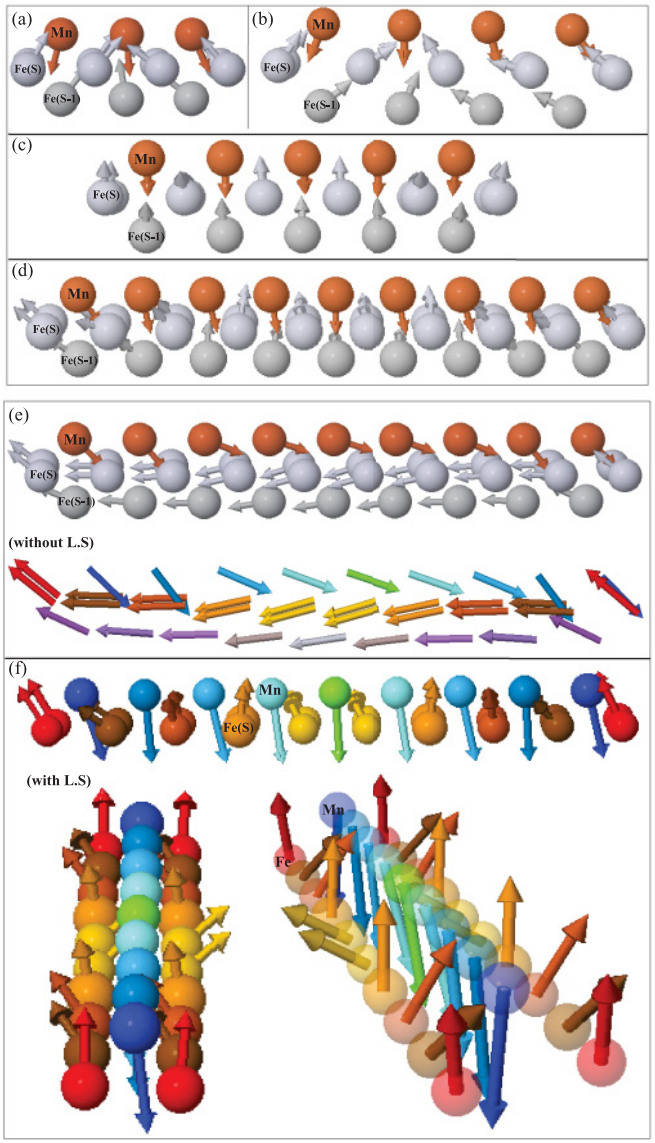

FIG. 4. (Color online) Noncollinear magnetic configurations for wires having (a) Mn_3, (b) Mn_4, (c) Mn_5, and (d) Mn_9 on Fe(001). (e) and (f) show the magnetic configurations for Mn_9 wire without and with spin-orbit coupling, respectively. In (f) the arrows are proportional to the local magnetic moments.

differing by a few meV/atom. Figures 4(c) and 4(d) reveal that the magnetic ordering displayed by these systems may be quite subtle, particularly for longer wires. We find very different magnetic orientations for the surface Fe atoms that have Mn atoms as first neighbors when we perform calculations with and without spin-orbit interaction. In the latter, shown in Fig. 4(e), we obtained a spin-density wave, characterized by a sinusoidal modulation with a period ≈2.5 nm, which corresponds to the Mn nanowire length. The Fe moments in the subsurface layer (S-1) display a similar behavior, but with smaller amplitude. The noncollinear magnetic configuration of the Mn moments resembles a damped wave, with the Mn moments at the corners being AF coupled to the nearest-neighbor Fe atoms situated underneath.

Calculations for longer wires taking into account spin-orbit coupling show a spin rotation, depicted in Fig. 4(f), that may be

caused by non-negligible contributions of the Dzyaloshinskii-Moriya interaction.[52,53] Along the Mn wire and their nearest-neighbor Fe sites the magnetic moments order as a helical spin spiral[54] with period approximately equal to the Mn wire length.

For systems in which Mn interdiffusion takes place (Fig. 3), our calculations show a canted antiferromagnetic alignment between the embedded and the absorbed Mn atoms. The directions of the nearest-neighbor Fe moments are almost perpendicular to the Mn ones. Nevertheless, we find that these magnetic configurations have higher energies in comparison with the collinear magnetic configurations (≈20 meV for the dimer and ≈100 meV for the trimer), indicating that Mn interdiffusion can stabilize the collinear configurations.

It is noteworthy that we did not find the even-odd effect reported in Ref. 55 for Mn nanochains adsorbed on fcc Fe(001), in which chains with an even number of Mn atoms always exhibit noncollinear magnetism, in contrast with those with odd numbers that display a collinear ferrimagnetic configuration. The distinct magnetic characteristics presented by Mn nanowires adsorbed on fcc and bcc Fe(001) surfaces arise from the very different competing pairwise exchange interactions that occur in these two systems.

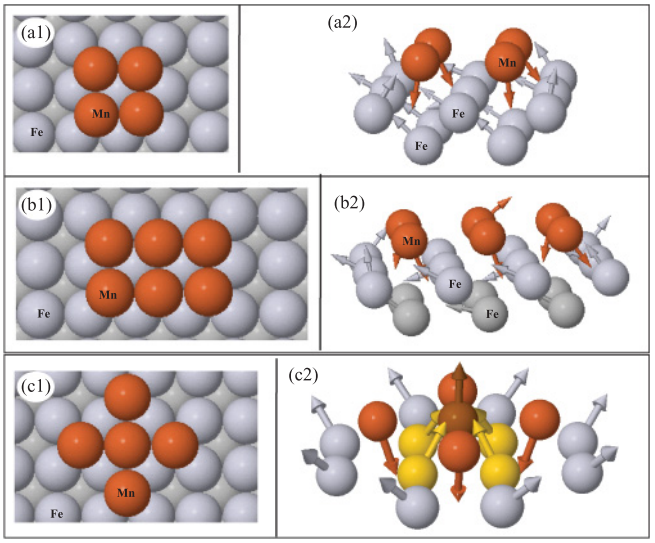

FIG. 5. (Color online) Magnetic configurations for Mn islands with (a) four (square), (b) six (rectangle), and (c) five (cross) atoms on Fe(001). (a1), (b1), and (c1) indicate the top views whereas (a2), (b2), and (c2) show the side views. The yellow balls in (c2) indicate Fe atoms closest to the central Mn site.

B. Mn nanostructures on Fe(001)

The morphology of a Mn nanostructure adsorbed on Fe(001) may play an important role in its magnetic characteristics. In order to investigate this effect, we have performed calculations, with spin-orbit coupling, for two-dimensional Mn islands with four (square), five (cross), and six (rectangle) atoms, as well as for a pyramid-shaped cluster consisting of five Mn atoms. These structures are depicted in Figs. 5 and 7. For the square-shaped Mn island shown in Fig. 5(a1), we find that the most stable magnetic state is the collinear $c(2 \times 2)$ ferrimagnetic spin arrangement, but it is nearly degenerate with the $p(2 \times 2) \uparrow$ configuration (here the $\uparrow$ label indicates that most Mn magnetic moments are parallel to the Fe substrate magnetization). Similar behavior was verified for the rectangle-shaped Mn cluster portrayed in Fig. 5(b1). For the cross-shaped Mn island with five atoms [Fig. 5(c1)], the most stable collinear magnetic configuration has the central Mn magnetic moment aligned antiparallel to the other Mn moments. The competition between exchange interactions and their long-range character yields several local minima in the energy landscape. The energies of the noncollinear magnetic states, shown in Fig. 5, are very similar to those associated with the collinear states. For the square- and rectangle-shaped Mn islands, we obtained a stable magnetic configuration in which the orientations of the Fe and Mn nearest-neighbor moments are almost antiparallel to each other when the Fe atom has only one Mn nearest neighbor, and almost perpendicular to each other when it has two Mn nearest neighbors [Figs. 5(a2) and (b2)]. Figure 5(c2) displays the noncollinear magnetic order of the Mn nanocluster with five atoms adsorbed on Fe(001). In this nontrivial magnetic structure the Mn and Fe magnetic moments rotate out of the surface plane, around the central Mn site, in a "lotus flower"-like spin configuration that resembles a half-skyrmion, i.e., a meron, topological object.[49,56] It is interesting to note that Heinze *et al.*[57] have reported the existence of a two-dimensional square lattice of skyrmions as the magnetic ground state of an Fe film on Ir(111) surface. The microscopic origin has been explained in terms of a complex interplay between exchange interactions of various orders and Dzyaloshinskii-Moriya interactions. Our finding of the complex magnetic structure reported in Fig. 5(c2) requires a similar analysis and will be done in a future communication.

These complex magnetic configurations may be explained by the pairwise exchange interactions involving the nanostructure Mn atoms ($J_{\mathrm{Mn-Mn}}$) as well as the coupling between a given Mn atom and the underlying Fe atoms ($J_{\mathrm{Mn-Fe}}$). Our results, presented in Fig. 6, were all calculated from the FM reference configuration. Similarly to the Mn nanowires, we obtained the following: (i) The coupling between nearest-neighbor Fe atoms ($J_{\mathrm{Fe-Fe}}$) is strong and positive, and decays relatively fast for farther neighbors; (ii) $J_{\mathrm{Mn-Mn}}$ and $J_{\mathrm{Mn-Fe}}$ have longer range and in some cases their magnitudes for nearest-neighbor moments are smaller than those between more distant neighbors; (iii) $J_{\mathrm{Mn-Fe}}$ depends not only on the Mn-Fe interatomic distance, but also on the number of Mn nearest neighbors of the Fe atom. We see in Fig. 6(d) that the value of $J_{\mathrm{Mn-Fe}}$ between nearest neighbors is negative if the Fe atom has only one Mn atom close to it, and positive when it has more than one Mn nearest neighbor. We also found that $J_{\mathrm{Mn-Mn}}$ is very sensitive to the number of Mn first and second (in plane) nearest neighbors (N_{Mn}). In Fig. 6(a) we see that the values of $J_{\mathrm{Mn-Mn}}$ range from -2.7 meV to $+8.2$ meV for Mn atoms that are one lattice parameter (a) apart. In Fig. 6(c) we show that $J_{\mathrm{Mn-Mn}}$, between Mn atoms separated by the same interatomic distance a, decreases very fast with N_{Mn}. For freestanding[58,59] and supporting Mn nanostructures on nonmagnetic substrates,[43,58,60,61] a sensitive dependence of the exchange interaction in Mn nanostrucutures on their environment has also been verified.

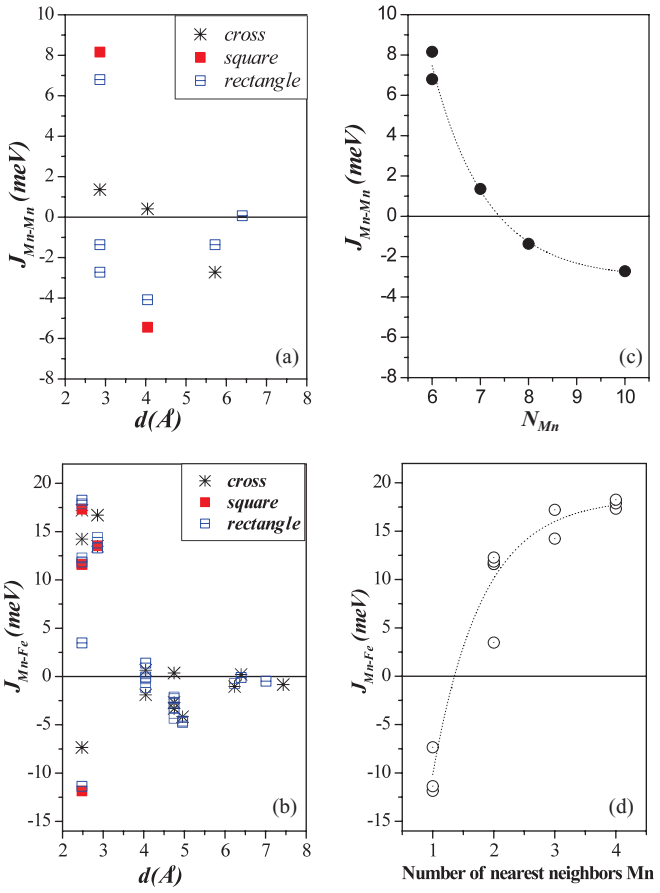

FIG. 6. (Color online) Pairwise exchange couplings calculated as functions of interatomic distances for different Mn islands adsorbed on Fe(001): (a) J_{Mn-Mn} and (b) J_{Mn-Fe}. The labels (i-j) (Fe or Mn) denote the sites i and j as depicted in Fig. 5. Panels (c) and (d) show the calculated values of J_{Mn-Mn} and J_{Mn-Fe} between nearest-neighbor sites as functions of N_{Mn} (see text), and the number of nearest-neighbor Mn atoms, respectively.

The values obtained for J_{Mn-Fe} and J_{Mn-Mn} provide a possible explanation to the magnetic configuration transition observed for submonolayer coverages of Mn adsorbed on Fe(001). As seen in Fig. 6, for low Mn coverages (small number of Mn neighbors), the FM Mn-Mn and AFM Mn-Fe coupling prevail. This is consistent with what has been observed in this limit, i.e., that the Mn moments are FM coupled to each other, but AF coupled with the Fe substrate magnetization.[1,7,8] For higher Mn coverages, as the number

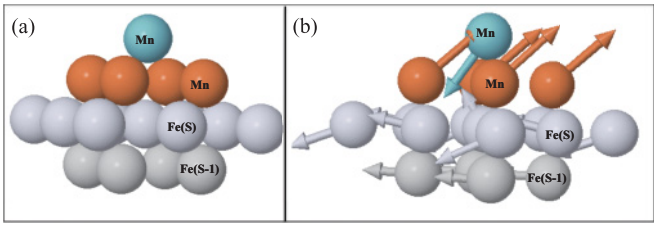

FIG. 7. (Color online) Magnetic configuration for Mn pyramid-shaped cluster adsorbed on Fe(001). The arrows are proportional to the local magnetic moments. S and S-1 denote the surface and subsurface Fe layers, respectively.

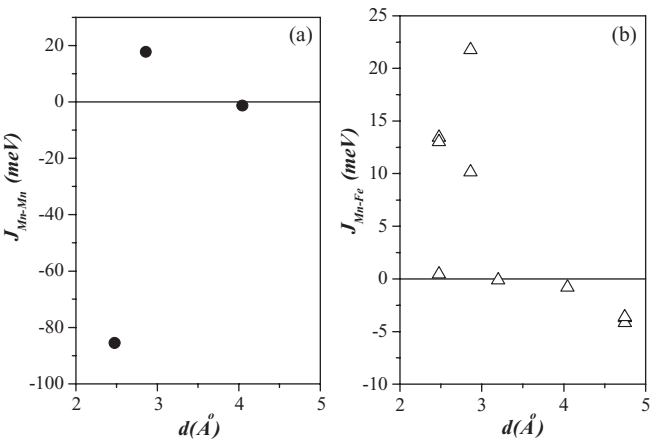

FIG. 8. Exchange coupling parameters (a) J_{Mn-Mn} and (b) J_{Mn-Fe} as a function of the distance between the sites, for the atoms displayed in Fig. 7.

of Mn neighbors increases, the Mn-Mn coupling switches to AFM, and the Mn-Fe coupling between nearest neighbors changes to FM, with some competition between interactions with further neighbors taking place. This may give rise to the canted in-plane AFM configuration observed in a monolayer of Mn on Fe(001), which orders almost perpendicular to the Fe substrate magnetization.[6]

For the Mn pyramid-shaped cluster adsorbed on Fe(001), shown in Fig. 7(a), the most stable collinear magnetic state exhibits a FM alignment of the Mn moments located in a same layer, as well as between the interface Mn and Fe moments, but an antiparallel ordering between Mn moments situated in different layers. The ground-state magnetic configuration obtained in our noncollinear calculations is shown in Fig. 7. The magnetic moment of the Mn atom situated on top of the pyramid is almost antiparallel to the Mn moments located at the interface with the Fe surface. These Mn moments are almost perpendicular to the neighboring Fe moments, in agreement with experimental[2,3] and theoretical[37] results for Mn overlayers on Fe(001). The exchange coupling calculated between first-neighbor Mn atoms (Fig. 8) is negative and very large in modulus, thus favoring a strong AF coupling between them. The amplitude of J_{Mn-Mn} decreases, oscillating between FM and AF, as the interatomic distance between Mn sites located in the same layer increases. The exchange interactions between Mn and Fe atoms across the interface are ferromagnetic for nearest neighbors, but becomes smaller and antiferromagnetic for more distant neighbors.

IV. CONCLUSION

We have studied several magnetic nanostructures in the form of wires and clusters of Mn adsorbed on an Fe(001) surface by first-principles density-functional calculations within the framework of noncollinear magnetism and spin-orbit interactions. We have found that the pairwise exchange interactions between neighboring Mn and Fe atoms in these systems depend not only on the interatomic distance, but strongly on the number of nearest neighbors. It is found that the stability of collinear or noncollinear magnetic ground states depends

on the degree of interdiffusion between Mn and Fe. A possible explanation of how the magnetic configurations evolve from a Mn adatom to Mn nanostructures or ultrathin films supported on Fe(001) has been presented. The energy landscape within the framework of collinear magnetism contains several minima giving rise to multiple magnetic configurations of competing energies. The allowance of noncollinear magnetism reveals a number of novel magnetic structures, including helical spin spirals in long Mn wires. Also, the Mn cross-shaped cluster with five atoms shows an intriguing noncollinear magnetic configuration, which can be described by topological structures, such as the half-skyrmion. The detailed analysis of these exotic magnetic structures by microscopic spin models having competing interaction terms is in progress.

ACKNOWLEDGMENTS

We acknowledge financial support from CNPq, CAPES, FAPESP, and FAPESPA, Brazil. The calculations were performed at the computational facilities of the LCCA, University of São Paulo, and of the CENAPAD at University of Campinas, SP, Brazil.

[1] Ch. Roth, Th. Kleemann, F. U. Hillebrecht, and E. Kisker, Phys. Rev. B **52**, R15691 (1995).
[2] T. K. Yamada, M. M. J. Bischoff, G. M. M. Heijnen, T. Mizoguchi, and H. van Kempen, Phys. Rev. Lett. **90**, 056803 (2003).
[3] U. Schlickum, N. Janke-Gilman, W. Wulfhekel, and J. Kirschner, Phys. Rev. Lett. **92**, 107203 (2004).
[4] T. G. Walker and H. Hopster, Phys. Rev. B **48**, R3563 (1993).
[5] D. A. Tulchinsy, J. Unguris, and R. J. Celotta, J. Magn. Magn. Mater. **212**, 91 (2000).
[6] C. Grazioli, D. Alfè, S. R. Krishnakumar, S. S. Gupta, M. Veronese, S. Turchini, N. Bonini, A. Dal Corso, D. D. Sarma, S. Baroni, and C. Carbone, Phys. Rev. Lett. **95**, 117201 (2005).
[7] J. Dresselhaus, D. Spanke, F. U. Hillebrecht, E. Kisker, G. van der Laan, J. B. Goedkoop, and N. B. Brookes, Phys. Rev. B **56**, 5461 (1997).
[8] O. Rader, W. Gudat, D. Schmitz, C. Carbone, and W. Eberhardt, Phys. Rev. B **56**, 5053 (1997).
[9] T. K. Yamada, E. Martínez, A. Vega, R. Robles, D. Stoeffler, A. L. Vázquez de Parga, T. Mizoguchi, and H. van Kempen, Nanotechnology **18**, 235702 (2007).
[10] W. Wulfhekel, U. Schlickum, and J. Kirschner, Microsc. Res. Tech. **66**, 105 (2005).
[11] A. Tange, C. Gao, W. Wulfhekel, and J. Kirschner, Phys. Rev. B **81**, 220404 (2010).
[12] S. T. Purcell, M. T. Johnson, N. W. E. McGee, R. Coehoorn, and W. Hoving, Phys. Rev. B **45**, 13064 (1992).
[13] S. K. Kim, Y. Tian, M. Montesano, F. Jona, and P. M. Marcus, Phys. Rev. B **54**, 5081 (1996).
[14] S. Andrieu, M. Finazzi, Ph. Bauer, H. Fischer, P. Lefevre, A. Traverse, K. Hricovini, G. Krill, and M. Piecuch, Phys. Rev. B **57**, 1985 (1998).
[15] M. M. J. Bischoff, T. K. Yamada, A. J. Quinn, and H. van Kempen, Surf. Sci. **501**, 155 (2002).
[16] T. K. Yamada, M. M. J. Bischoff, T. Mizoguchi, and H. van Kempen, Surf. Sci. **516**, 179 (2002).
[17] P. Torelli, F. Sirotti, and P. Ballone, Phys. Rev. B **68**, 205413 (2003).
[18] D. Spisák and J. Hafner, Surf. Sci. **601**, 4348 (2007).
[19] J. Hafner and D. Spisak, Phys. Rev. B **72**, 144420 (2005).
[20] T. Asada, S. Blügel, G. Bihlmayer, S. Handschuh, and R. Abt, J. Appl. Phys. **87**, 5935 (2000).
[21] S. Handschuh and S. Blügel, Solid State Commun. **105**, 633 (1998).
[22] O. Elmouhssine, G. Moraitis, C. Demangeat, and J. C. Parlebas, Phys. Rev. B **55**, R7410 (1997).
[23] D. Spisak and J. Hafner, Phys. Rev. B **55**, 8304 (1997).
[24] S. Mirbt, O. Eriksson, B. Johansson, and H. L. Skriver, Phys. Rev. B **52**, 15070 (1995).
[25] E. Martínez, A. Vega, R. Robles, and A. L. Vázquez de Parga, Phys. Lett. A **337**, 469 (2005).
[26] R. Wu and A. J. Freeman, Phys. Rev. B **51**, 17131 (1995).
[27] B. Nonas, K. Wildberger, R. Zeller, and P. H. Dederichs, Phys. Rev. Lett. **80**, 4574 (1998); J. Magn. Magn. Mater. **165**, 137 (1997).
[28] J. T. Lau, A. Fohlisch, R. Nietubyc, M. Reif, and W. Wurth, Phys. Rev. Lett. **89**, 057201 (2002)
[29] S. Rusponi, T. Cren, N. Weiss, M. Epple, P. Buluschek, L. Claude, and H. Brune, Nat. Mater. **2**, 546 (2003).
[30] W. Kuch, Nat. Mater. **2**, 505 (2003).
[31] J. A. Stroscio and R. J. Celotta, Science **306**, 242 (2004).
[32] Y. Yayon, V. W. Brar, L. Senapati, S. C. Erwin, and M. F. Crommie, Phys. Rev. Lett. **99**, 067202 (2007).
[33] T. Balashov, T. Schuh, A. F. Takács, A. Ernst, S. Ostanin, J. Henk, I. Mertig, P. Bruno, T. Miyamachi, S. Suga, and W. Wulfhekel, Phys. Rev. Lett. **102**, 257203 (2009).
[34] A. J. Heinrich, J. A. Gupta, P. Lutz, and D. M. Eigler, Science **306**, 466 (2004).
[35] A. T. Costa Jr., R. B. Muniz, and D. L. Mills, Phys. Rev. Lett. **94**, 137203 (2005).
[36] N. N. Negulyaev, V. S. Stepanyuk, W. Hergert, and J. Kirschner, Phys. Rev. Lett. **106**, 037202 (2011).
[37] H. Tan, E. Martínez, A. Vega, V. M. Uzdin, R. Robles, and G. Borstel, Surf. Sci. **603**, 2537 (2009).
[38] P. R. Peduto, S. Frota-Pessôa, and M. S. Methfessel, Phys. Rev. B **44**, 13283 (1991).
[39] S. Frota-Pessôa, Phys. Rev. B **46**, 14570 (1992).
[40] O. K. Andersen, O. Jepsen, and D. Glötzel, *Highlights of Condensed-Matter Theory* (North Holland, Amsterdam, 1985).
[41] R. Haydock, *Solid State Physics* (Academic, New York, 1980), Vol. 35.
[42] A. Bergman, L. Nordström, A. B. Klautau, S. Frota-Pessôa, and O. Eriksson, Phys. Rev. B **73**, 174434 (2006).
[43] A. Bergman, L. Nordström, A. B. Klautau, S. Frota-Pessôa, and O. Eriksson, Phys. Rev. B **75**, 224425 (2007).
[44] U. von Barth and L. A. Hedin, J. Phys. C **5**, 1629 (1972).
[45] N. Beer and D. Pettifor, *The Electronic Structure of Complex Systems* (Plenum, New York, 1984).
[46] A. I. Liechtenstein, M. I. Katsnelson, V. P. Antropov, and V. A. Gubanov, J. Magn. Magn. Mater. **67**, 65 (1987).
[47] S. Frota-Pessôa, R. B. Muniz, and J. Kudrnovský, Phys. Rev. B **62**, 5293 (2000).

[48]M. Ezawa, Phys. Rev. B **83**, 100408 (2011).
[49]*The Multifaceted Skyrmions*, edited by G. E. Brown and M. Rho (World Scientific, Singapore, 2010).
[50]X. Z. Yu, Y. Onose, N. Kanazawa, J. H. Park, J. H. Han, Y. Matsui, N. Nagaosa, and Y. Tokura, Nature **465**, 901 (2010).
[51]U. K. Rössler, A. N. Bogdanov, and C. Pfleidere, Nature **442**, 797 (2006).
[52]I. E. Dzyaloshinskii, Sov. Phys. JETP **5**, 1259 (1957).
[53]T. Moriya, Phys. Rev. **120**, 91 (1960).
[54]M. Bode, M. Heide, K. von Bergmann, P. Ferriani, S. Heinze, G. Bihlmayer, A. Kubetzka, O. Pietzsch, S. Blügel, and R. Wiesendanger, Nature **447**, 190 (2007).
[55]S. Lounis, P. H. Dederichs, and S. Blügel, Phys. Rev. Lett. **101**, 107204 (2008).
[56]S. John, M. Berciu, and A. Golubentsev, Europhys. Lett. **41**, 31 (1998).
[57]S. Heinze, K. von Bergmann, M. Menzel, J. Brede, A. Kubetzka, R. Wiesendanger, G. Bihlmayer, and S. Blügel, Nat. Phys. **7**, 713 (2011).
[58]F. Schubert, Y. Mokrousov, P. Ferriani, and S. Heinze, Phys. Rev. B **83**, 165442 (2011).
[59]M. Zelený, M. Sob, and J. Hafner, Phys. Rev. B **80**, 144414 (2009).
[60]P. Mavropoulos, S. Lounis, and S. Blügel, Phys. Status Solidi B **247**, 1187 (2010).
[61]M. S. Ribeiro, G. B. Corrêa Jr., A. Bergman, L. Nordström, O. Eriksson, and A. B. Klautau, Phys. Rev. B **83**, 014406 (2011).